Yong Du[a], Jiong Wang[a], Jingrui Zhao[a], Julius Clemens Schuster[b], Franz Weitzer[b], Rainer Schmid-Fetzer[c], Munekazu Ohno[c], Honghui Xu[a], Zi-kui Liu[d], Shunli Shang[d], Wenqing Zhang[e]

[a] State Key Laboratory of Powder Metallurgy, Central South University, Hunan, China
[b] Innovative Materials Group, University of Vienna, Vienna, Austria
[c] Clausthal University of Technology, Institute of Metallurgy, Clausthal-Zellerfeld, Germany
[d] Department of Materials Science and Engineering, Pennsylvania State University, PA, USA
[e] State Key Laboratory of High Performance Ceramics and Superfine Microstructure, Shanghai Institute of Ceramics, Chinese Academy of Sciences, Shanghai, China

Reassessment of the Al–Mn system and a thermodynamic description of the Al–Mg–Mn system

Dedicated to Prof. Dr. Gunnar Eriksson on the occasion of his 65th birthday

A thermodynamic optimization for the Al–Mn system is performed by considering reliable literature data and newly measured phase equilibria on the Al-rich side. Using X-ray diffraction, differential thermal analysis, and scanning electron microscopy with energy dispersive X-ray spectroscopy methods, the melting behavior of λ-Al_4Mn was correctly elucidated, and two invariant reactions associated with λ-Al_4Mn ($L + \mu\text{-}Al_4Mn \leftrightarrow \lambda\text{-}Al_4Mn$ at $721 \pm 2\,°C$ and $L + \lambda\text{-}Al_4Mn \leftrightarrow Al_6Mn$ at $704 \pm 2\,°C$) are observed. The model $Al_{12}Mn_4(Al, Mn)_{10}$ previously used for Al_8Mn_5 was modified to be $Al_{12}Mn_5(Al, Mn)_9$ based on crystal structure data. In addition, the high-temperature form of $Al_{11}Mn_4$ is included in the assessment. Employing fewer adjustable parameters than previous assessments, the present description of the Al–Mn system yields a better overall agreement with the experimental phase diagram and thermodynamic data. The obtained thermodynamic description for the Al–Mn system is then combined with those in the Al–Mg and Mg–Mn systems to form a basis for a ternary assessment. The thermodynamic parameters for ternary liquid and ternary compound $Mn_2Mg_3Al_{18}$ (τ) are evaluated on the basis of critically assessed experimental data. The enthalpy of formation for τ resulting from CALPHAD (CALculation of PHAse Diagrams) approach agrees reasonably with that via first-principles methodology. Comparisons between the calculated and measured phase equilibria in the Al–Mg–Mn system show that the accurate experimental information is satisfactorily accounted for by the present description. A reaction scheme for the whole ternary system is presented for practical applications.

Keywords: Phase diagram Al–Mg–Mn; Thermodynamic calculations; X-ray diffraction; Differential thermal analysis

1. Introduction

The Al–Mn system is of special interest to the aluminum industry since most commercial Al alloys contain small amounts of Mn. For Mg alloys, addition of a small amount of Mn yields an improvement of corrosion resistance and enhancement of grain refinement. Consequently, the ternary Al–Mg–Mn system is one of the most important systems for the development of both Al- and Mg-based alloys. Information on phase equilibria and thermodynamic properties is essential to design solidification processes and subsequent heat treatments in order to improve the properties of these materials.

The thermodynamic parameters for the Al–Mg [1] and Mg–Mn [2] systems are well established. The Al–Mn system is a very complex one in which a large number of intermetallic phases have been found. Table 1 lists the crystallographic data for the solid phases reported so far [3–5]. The metastable phases, icosahedral i-AlMn, decagonal T-AlMn, π-Al_4Mn, $Al_{10}Mn_3$, $Al_{78}Mn_{22}$, reported by Kreiner and Franzen [5], are also listed in this table. Several assessments [6–8] are available for the Al–Mn system. These evaluations used the model $Al_{12}Mn_4(Al, Mn)_{10}$ for Al_8Mn_5. In accordance with crystallography [4], the model should be corrected to be $Al_{12}Mn_5(Al, Mn)_9$. The thermodynamic assessment by Liu et al. [7] improved the modeling of Jansson [6] by considering their own experimental phase equilibria over the temperature range of 800 to 1200 °C and the composition range of 50 to 80 at.% Mn. A combination of the diffusion couple technique, optical metallography (OM), X-ray diffraction (XRD), and differential scanning calorimetry (DSC) was employed by them [7], providing accurate phase equilibrium data for the ranges mentioned above. However, several aspects could be improved in the evaluation by Liu et al. [7]. One is that the experimental liquidus temperature in the composition range of 3 to 15 at.% Mn [9–11] is higher by about 10 to 15 °C than the computed

Table 1. Crystallographic data for the solid phases in Al–Mg–Mn system.

Phase/Temperature Range (°C)	Pearson Symbol/ Space Group/Prototype	Lattice Parameters (pm)	Comments/References
(Al) <660.5	cF4 $Fm\bar{3}m$ Cu	a = 404.88	[3]
(Mg) <650	hP2 $P6_3/mmc$ Mg	a = 320.89 c = 521.01	[3]
(δMn) 1246–1138	cI2 $Im\bar{3}m$ W	a = 308.1	[3]
(γMn) 1138–1087	cF4 $Fm\bar{3}m$ Cu	a = 386.2	[3]
(βMn) <1087–707	cP20 $P4_132$ βMn	a = 631.5	[3]
(αMn) <707	cI58 $I\bar{4}3m$ αMn	a = 891.39	[3]
β-AlMg (Al_3Mg_2) ≤451	cF1168 $Fd\bar{3}m$ Al_3Mg_2	a = 2816 to 2824	[3]
γ-AlMg ($Al_{12}Mg_{17}$) <464	cI58 $I\bar{4}3m$ αMn	a = 1054.38	[3]
ε-AlMg ($Al_{30}Mg_{23}$) 410–250	hR159 $R\bar{3}h$ $Mn_{44}Si_9$	a = 1282.54 c = 2174.78	[3]
$Al_{12}Mn$ <512	cI26 Im3 $Al_{12}W$	a = 750.7	[3]
Al_6Mn <703	oC28 Cmcm Al_6Mn	a = 754.5(2) b = 649.0(3) c = 868.1(2)	[3]
λ-Al_4Mn <721	hP586 $P6_3/m$	a = 2838.2 c = 1238.9	[5]
μ-Al_4Mn <922	hP574 $P6_3/mmc$ Al_4Mn	a = 1998(1) c = 2467.3(3)	[5]
$HTAl_{11}Mn_4$ (Al_3Mn) 1002–905	oP156 $Pn2_1a$ Al_3Mn	a = 1485.4 b = 1242.2 c = 1254.0	[5]
$LTAl_{11}Mn_4$ ≤914	aP15 $P\bar{1}$ $Al_{11}Mn_4$	a = 509.5(4) b = 887.9(8) c = 505.1(4) α = 89.35° β = 1004.47° γ = 105.08°	[3]
Al_8Mn_5 <1046	hR26 R3m Al_8Cr_5	a = 1266.7(3) c = 794.2(2) a = 1259.8(2) c = 792.1(2)	[4] at 38.5 at.% Mn [4] at 46.5 at.% Mn
γ-AlMn 1185–849	cI2 $Im\bar{3}m$ W	a = 306.3(3)	[4]
ε-AlMn 1281–823	hP2 $P6_3/mmc$ Mg	a = 269.8 c = 437.0	[3]

Table 1. (continued)

Phase/Temperature Range (°C)	Pearson Symbol/ Space Group/Prototype	Lattice Parameters (pm)	Comments/References
τ-$Al_{18}Mg_3Mn_2$	cF184 $Fd\bar{3}m$ $Al_{18}Mg_3Cr_2$	a = 1452.9	[3]
π-Al_4Mn	oC152 Cmcm	a = 770 b = 1360 c = 1240	metastable [5]
i-AlMn	$Pm\bar{3}\bar{5}$ icosahedral	a = 650.5	metastable [5] formed from the metastable liquid by a first order transition
T-AlMn	$P10_2/mmc$ decagonal	a_1 = 391.2 a_2 = 1240	metastable [5] fromed in melt-spun ribbons
$Al_{10}Mn_3$	hP26 $P6_3/mmc$ Al_5Co_2	a = 754.3 c = 789.8	metastable [3] formed from the liquid during cooling and probably also during decomposiont of super-saturated (Al)
τ-AlMn	tP2 P4/mmm AuCu	a = 277 c = 354	metastable [5] formed from the high-temperature phase ε-AlMn region during cooling at rates of about 10 $K \cdot s^{-1}$ or retained ε-AlMn at low temperature

one [7]. The second aspect concerns the decomposition of $Al_{11}Mn_4$ into μ-Al_4Mn and Al_8Mn_5 at low temperature. This decomposition has not been experimentally observed and it is considered as a mathematical artifact, as pointed out by Ohno and Schmid-Fetzer [8]. An additional uncertainty with the modeling of Liu et al. [7] is due to the contradictory report on the melting behavior of λ-Al_4Mn. Due to this debate, this phase was not included in the modeling due to Liu et al. [7]. Early experimental work [9, 10, 13] established that λ-Al_4Mn is formed by the incongruent melting of Al_6Mn into liquid (L) + λ-Al_4Mn at 705 °C < T < 710 °C upon heating Al_6Mn. Upon cooling, the formation of λ-Al_4Mn from L or from the L + μ-Al_4Mn phase region was convincingly observed in the annealing and quench experiments [10, 13]. Subsequent investigation by Murray [14], however, indicated that λ-Al_4Mn is not in equilibrium with liquid Al–Mn alloys and it is formed via the reaction Al_6Mn + μ-Al_4Mn ↔ λ-Al_4Mn. This interpretation was not challenged, although the thermal effect for this solid state reaction was not corroborated by Robinsion et al. [15]. Modifying the published thermodynamic parameter [7] for $Al_{11}Mn_4$, Ohno and Schmid-Fetzer [8] removed the unusual decomposition feature for this phase. But, the other shortcomings mentioned above still remain. Thus, further experiment is necessary to identify the melting nature of λ-Al_4Mn and the thermodynamic description for the Al–Mn system needs to be refined in order to get a better agreement with the experimental data.

The Al–Mg–Mn ternary system is one of the important ternary systems in Al- and Mg- based commercial alloys. It is well known that an addition of a small amount of Mn results in improvement of corrosion resistance [16] and grain refinement has been observed [17]. The phase equilibra in the Al–Mg–Mn system have been mainly measured close to the Al–Mg side. These experimental data were reviewed by Ran [18] and Ohno and Schmid-Fetzer [8]. Two thermodynamic descriptions for the Al–Mg–Mn system are available in the literature. One is valid only in the Al-rich part [19], the other is concentrated on Mg-rich alloys [8].

The major purpose of the present work is to obtain an accurate thermodynamic description of the Al–Mn system by using reliable literature data, supplemented with key experiments in the Al-rich side with a desire to identify the melting nature of λ-Al_4Mn. The description for this binary system is then combined with the thermodynamic parameters in Al–Mg [1] and Mg–Mn [2] to synthesize a thermodynamic description of the ternary system. In ternary modeling, our focus is placed on both the Al- and Mg-rich sides.

2. Experimental data in the literature for the Al–Mn and Al–Mg–Mn systems

2.1. The Al–Mn system

The phase equilibria and thermodynamic properties in the Al–Mn system have been subjected to numerous investigations. The experimental data prior to 1987 were reviewed by McAlister and Murray [20]. Subsequently, the Al–Mn system was modeled by Jansson [6] and Liu et al. [7]. All of the experimental data reviewed by them, together with those [21–26] not covered by them and later published values [11, 12, 15], are considered in the present optimization. All of these experimental data [9–15, 21–40] are summarized in Table 2. Also included in the table is the present experiment. As will be shown later these new measurements clarify the melting behavior of λ-Al_4Mn undoubtedly and yield a modified version of the phase equilibria in the Al-rich corner. To conserve space, only the experimental data not included in the recent evaluation [7] are critically evaluated.

Kuznetsov et al. [21] measured the solubility of Mn in (Al) in a wide temperature range of 250 to 600 °C by means of XRD, OM, electrical resistance measurement (ER), and

Table 2. Summary of the experimental phase diagram and thermodynamic data in the Al–Mn system.

Type of experimental data	Experimental method*	Reference	Quotation[a]
Phase diagram in Al-rich side	EL, OM, TA, XRD	[9]	–
Phase diagram from 10 to 45 at.% Mn	DTA, OM, XRD	[10]	+
Phase diagram from 7.5 to 9 wt.% Mn	DTA	[11]	+
Phase diagram from 3 to 6 wt.% Mn	DTA	[12]	+
Phase diagram from 33 to 45 at.% Mn	DM, OM, XRD	[13]	+
Phase diagram from 12 to 22.5 at.% Mn	DTA, TEM, XRD	[14]	–
Phase diagram below 11 at.% Mn	DTA	[15]	+
Phase diagram below 37 wt.% Mn	OM, TA, XRD	[28]	–
Phase diagram from 47 to 60 at.% Mn	XRD, OM	[31]	–
Phase diagram from 40 to 95 at.% Mn	XRD, TA	[32]	–
Phase diagram from 29.5 to 100 at.% Mn	XRD, TA, OM	[33]	+
Phase diagram from 29.5 to 97.5 at.% Mn	OM, HM, TA	[34]	+
Phase diagram from 50 to 80 at.% Mn	DSC, HM, OM, XRD	[40]	+
Phase diagram from 5 to 20 at.% Mn	DTA, OM, XRD	This work	+
Solubility of Mn in (Al)	ER, HM, OM, XRD	[21]	+
Solubility of Mn in (Al)	EPMA	[22]	+
Solubility of Mn in (Al)	XRD	[25]	+
Solubility of Mn in (Al)	PFA	[26]	+
Solubility of Mn in (Al)	EL, OM	[27]	–
Solubility of Mn in (Al)	OM	[29]	–
Solubility of Mn in (Al)	XRD	[30]	+
Solubility of Mn in (Al)	ER, OM	[36]	+
Activities of Al and Mn from 1250 to 1550 K	KMS	[23]	+
Activity of Mn in liquid at 1297 °C	emf	[37]	+
Activity of Mn at 902 °C (42 to 55 at.% Mn)	KMS	[39]	–
Enthalpy of formation at 25 °C	DRC	[24]	+
Enthalpy of formation at 25 °C	Calorimetry	[35]	–
Enthalpy of mixing for liquid at 1626 K	Calorimetry	[38]	+

[a] indicates whether the data are used or not used in the optimization: +, used; –, not used.
* DM = density measurement; DRC = direct reaction calorimetry; DSC = differential scanning calorimetry; DTA = differential thermal analysis; EL = electrical conductivity; emf = electron motive force; EPMA = electron probe microanalysis; ER = electrical resistance; HM = hardness measurement; KMS = Knudsen mass spectrometry; OM = optical microscopy; PFA = phenol filtrate analysis; TA = thermal analysis; TEM = transmission electron microscopy, XRD = X-ray analysis.

hardness measurement (HM) techniques. The results from different methods are consistent with each other, and thus are included in the present optimization. The solubility of Mn in (Al) was determined by Minamino et al. [22], who performed the electron probe microanalysis (EPMA) measurement of the alloys quenched after annealing at known temperatures and pressures. Sigli [25] reported the solubility of Mn in (Al) from 550 to 650 °C. Based on the phenol filtrate analysis method, Matuo et al. [26] determined the solid solubility curve of Mn in (Al). The experimental data reported by three groups of authors [22, 25, 26] are in good agreement with those from Kuznetsov et al. [21]. As a result, they are utilized in the present optimization. The use of these accurate experimental data in thermodynamic optimization is expected to yield a more accurate solubility for Mn in (Al) than the previous assessment from Liu et al. [7], who neglected these data. Three groups of investigators [11, 12, 15] measured the liquidus temperatures in the Al-rich part using the Smith thermal analysis method [15], which results in the sample being in a condition close to equilibrium throughout thermal analysis and minimizes non-equilibrium effects such as supercooling. Consequently, these reported liquidus temperatures are used in the present optimization.

Using Knudsen cell mass spectrometry, Chastel et al. [23] determined the activities of both Al and Mn in the temperature range of 1250 to 1550 K. The enthalpies of formation for two alloys (Al_2Mn_3 and $AlMn_4$) were measured by Meschel and Kleppa [24] using direct synthesis calorimetry. These experimental thermodynamic data are utilized in the present modeling for the purpose of refining the thermodynamic parameters from Liu et al. [7], who did not take into account the two pieces of information.

2.2. The Al–Mg–Mn system

The Al–Mg–Mn system has mainly been investigated close to the Al–Mg side. All of the literature data [41–48] on Mg-rich phase equilibria were critically reviewed by Ohno and Schmid-Fetzer [8], who found that the experimental data from [41, 43, 48] are consistent with each other. As a consequence, these experimental data are included in the optimization of thermodynamic parameters.

Several groups of authors [49–60] contributed to the measurement of phase equilibria in the Al-rich corner. By means of metallography and thermal analysis and in some cases supplemented with annealing experiments and subsequent XRD, Leemann [49] established the phase relationships in the composition ranges of 0–35.5 wt.% Mg and 0–12 wt.% Mn. Based on XRD analysis of an alloy (Al-16.28 wt.% Mg-4.26 wt.% Mn), Hofmann [50] found a metastable eutectic of (Al), Al_3Mg_2 and Al_4Mn in the Al corner. Using the ER method, Fahrenhorst and Hofmann [51] determined the joint solubilities of Mg and Mn in (Al)

at 500, 550, and 600 °C. Butchers et al. [52] investigated the liquidus surface in Al-rich part with up to 5 wt.% Mg and 2 wt.% Mn on the basis of microstructure observation. Following the same method, Little et al. [53] determined the joint solubility of Mg and Mn in (Al) at 500 °C. Based on the data of Leemann [49] and his own experimental data, Mondolfo [54] constructed the equilibrium diagrams for the Al corner. However, any detail on the experimental procedure was not mentioned by Mondolfo [54]. Butchers and Hume-Rothery [55] determined the solidus isotherms and the isothermal section at 630 °C by observation of incipient melting and microstructure. The partial isothermal section at 400 °C within the composition ranges of 0 to 40 wt.% Mg and 0 to 25 wt.% Mn was established by Wakeman and Raynor [56] using optical microscopy. The 400, 450, and 550 °C isothermal sections in the Al-rich side were determined by Ohnishi et al. [57, 58] employing XRD and metallography. The ternary compound $MnMg_2Al_{10}$ (τ) was first found by Wakeman and Raynor [56] using metallographic observation and XRD. The crystal structure of τ was determined by Ohnishi et al. [57] and Fun et al. [59], who refined its stoichiometry to be $Mn_2Mg_3Al_{18}$. Among the experimental data reported so far for the Al-rich corner, the data reported in [51, 55–58, 60] are consistent with each other. Consequently, they are utilized in the present thermodynamic optimization.

3. Experimental investigation in the Al-rich side of the Al–Mn system

3.1. Experimental procedure

Since there is a dispute on the melting behavior of λ-Al_4Mn among the literature data, accurate experiment is performed in the present work to clarify this discrepancy. Another reason to conduct new experiments is that even the recent measurements [11, 12, 15] only provide limited experimental data on liquidus temperatures in the composition range of 5 to 20 at.% Mn. The published liquidus temperatures in this range are rather scattered.

The starting materials used for the present investigation are 99.999 wt.% purity Al-rods and 99.95 wt.% purity Mn-pieces (both from Alfa Aesar Johnson Matthey GmbH & Co KG, Karlsruhe, Germany). Alloys with weights between 1 and 2 g were prepared by melting the Al-rods and Mn pieces with an arc furnace in an ambient atmosphere of 99.998 % purity Ar. The vacuum inside this arc furnace was pumped below $\approx$5 Pa before the purge with Ar. In total 9 alloys were prepared within the composition range of 5 to 20 at.% Mn. All buttons were cut into several pieces. One piece was left in the as-cast state and the other pieces were annealed at temperatures ranging from 620 °C (4 days) to 750 °C (2 days). For these heat treatments the specimens were placed in Al_2O_3 crucibles and sealed in evacuated quartz tubes. In order to identify the effect of contamination with traces of Si, which potentially could occur during the heat treatment, two representative alloys (Al-13 at.% Mn and Al-16 at.% Mn) were placed in Y_2O_3 stabilized ZrO_2 crucibles and sealed in Ta cylinders, which in turn were sealed in quartz. All samples were quenched from the equilibration temperature by rapid submersion in cold water.

The phase identification was performed by means of XRD (model G670, Huber Diffraktionstechnik GmbH, Rimsting, Germany) using Cu-Kα_1 radiation with Si as an internal standard. The phase compositions were measured with scanning electron microscopy with energy dispersive X-ray spectroscopy (SEM/EDX) (model DSM692, C. Zeiss AG, Oberkochen, Germany). Conventional matrix correction, which treats the deviation from linearity by including the effects of atomic number (Z), absorption (A) and fluorescence (F) (ZAF), was utilized to calculate the compositions from the measured X-ray intensities.

Differential thermal analysis (DTA, DTA 701L, Bähr Thermoanalyse GmbH, Germany) measurements of the alloys were carried out in Al_2O_3 crucibles under a flow of pure Ar. Most measurements were conducted between room temperature and 1200 °C with a heating and cooling rate of 5 K · min^{-1}. In order to detect the effect of heating rate on the kinetics of λ-Al_4Mn formation, DTA measurements with heating rates of 2, 5, and 10 K · min^{-1} are performed for the representative alloy Al-12.5 at.% Mn. The temperature was measured with Pt–Pt/Rh thermocouples and calibrated to the melting temperatures of Al (660.3 °C), Ag (961.8 °C), Au (1064.2 °C), Si (1413.9 °C), Ni (1455.2 °C), and Co (1494.9 °C). The accuracy of the temperature measurement was estimated to be ±2 °C. The invariant reaction temperatures were determined from the onset of the thermal effects during the heating step, and

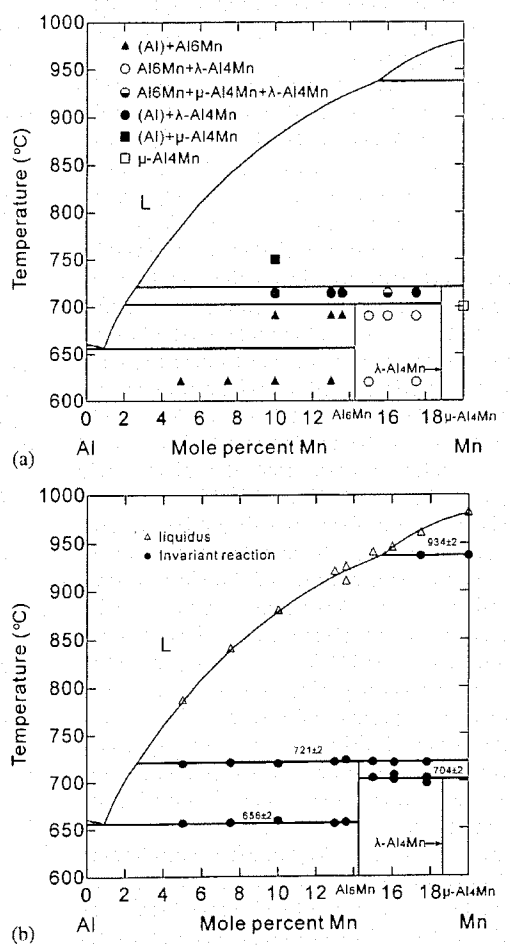

Fig. 1. Al-rich part of the Al–Mn phase diagram. (a) Derived from equilibration and quench experiments, (b) Derived from differential thermal analysis.

the offset temperatures of the last thermal effect on heating were taken for the liquidus.

3.2. Experimental results

Figure 1a shows the phase relation in the Al-rich side of the Al–Mn system derived from XRD analysis and microstructure observation of the equilibrated and quenched alloys. The DTA measurement of the same alloys yields the phase equilibrium as shown in Fig. 1b. As can be seen from Fig. 1, the phase relations resulting from each set of data contradict each other. XRD and microstructure observation indicate the existence of a phase field L + λ-Al_4Mn, while the DTA data suggest no existence of such a phase field. Thus one of the experimental methods must yield misleading data.

To ascertain if the results based on XRD and microstructure observation are reliable, the following aspects were carefully checked: (I) phase identification, (II) calibration of annealing temperature, (III) metastable phenomenon of λ-Al_4Mn, (IV) in-situ equilibrium resulting from quenching, and (V) contamination of the prepared alloys. It was found that nothing was wrong with phase identification and calibration of temperature and there was no contamination during the preparation of alloys. In addition, it was demonstrated that λ-Al_4Mn is a stable phase and the quenched alloy represents the in-situ equilibria at high temperatures. Thus, there is no reason to doubt the results based on XRD and microstructure observation.

What could be possible reasons for the misleading results in the DTA experiments? We focused on the kinetics of the reaction $Al_6Mn \rightarrow L + \lambda\text{-}Al_4Mn$ in detail. In order to investigate the kinetics associated with the formation of λ-$MnAl_4$, time-dependent annealing and quench experiments were performed for the alloy Al-12.5 at.% Mn annealed at 712 °C for 5, 50, 100, and 500 min, followed by water-quenching. XRD analysis shows that no trace of λ-Al_4Mn was formed within the first 50 min and even after 500 min the transformation was not complete. At a heating rate of 5 $K \cdot min^{-1}$, it takes only 12 min to heat the alloy from 690 °C, where Al_6Mn is still found even after prolonged annealing, to 750 °C, where L + μ-Al_4Mn is observed to coexist. Reducing the heating rate to 2 $K \cdot min^{-1}$ and assuming the unlikely case, that the phase field L + λ-Al_4Mn ranges from 690 °C to 750 °C, the phase λ-Al_4Mn has only 30 min to form or will not be detected by DTA. This evidence suggests that the formation of λ-Al_4Mn during incongruent melting of Al_6Mn is a slow nucleation controlled process. This nucleation barrier is responsible for the erroneous conclusions from data obtained by dynamic methods such as DTA. Care should be taken to check the general consistency of the phase diagram data obtained from different experimental methods. The present work indicates that although DTA is an effective approach to measure phase transition temperatures, it could yield erroneous results due to slow kinetics (such as a nucleation barrier) of reactions during measurement.

Alloys containing Al_6Mn + λ-Al_4Mn after equilibration at 620 or 690 °C show in the temperature interval between 690 °C and 750 °C the occurrence of two invariant reactions at 704 ± 2 °C and at 721 ± 2 °C, according to DTA measurement. Equilibrated alloys containing (Al) + Al_6Mn, however, give rise to the latter peak only. This is understandable since in the former case λ-Al_4Mn already exists and it could act as the nucleation sites for the formation of subsequent λ-Al_4Mn.

4. Thermodynamic modeling

4.1. CALPHAD approach

In the present modeling, the thermodynamic parameters in the Al–Mg and Mg–Mn systems are taken from Liang et al. [1] and Gröbner et al. [2], respectively. Figures 2 and 3 show the calculated Al–Mg and Mg–Mn phase diagrams, respectively. The Al–Mn system is reassessed in the present work by incorporating the literature data not covered by Liu et al. [7] and the present experimental data. The two phases λ-Al_4Mn and HT-$Al_{11}Mn_4$ (high-temperature form of $Al_{11}Mn_4$), which are included in the phase diagram assessed by McAlister and Murray [20] but neglected in the modeling by Liu et al. [7], are considered in the present optimization. Based on the crystal structure data, λ-Al_4Mn and HT-$Al_{11}Mn_4$ are described by the models $Al_{461}Mn_{107}$ [5] and $(Al,Mn)_{29}Mn_{10}$ [61, 62], respectively. In addition, the previous model $Al_{12}Mn_4(Al,Mn)_{10}$ [6–8] used for Al_8Mn_5 is modified in order to reflect its crystallography [4]. In accordance with the crystal structure data, this phase should be modeled with $Al_{12}Mn_5(Al,Mn)_9$. According to the sublattice model [63, 64], the Gibbs energy of Al_8Mn_5 per mole of atom is given by the following expression:

$$G_m^{Al_8Mn_5} - H^{SER} = y'''_{Al} \cdot G^{0,Al_8Mn_5}_{Al:Mn:Al} + y'''_{Mn} \cdot G^{0,Al_8Mn_5}_{Al:Mn:Mn}$$

$$+\frac{9}{26} \cdot R \cdot T(y'''_{Al} \cdot \ln y'''_{Al} + y'''_{Mn} \cdot \ln y'''_{Mn})$$

$$+ y'''_{Al} \cdot y'''_{Mn} \cdot \left[L^0_{Al:Mn:Al,Mn} + L^1_{Al:Mn:Al,Mn}\left(y'''_{Al} - y'''_{Mn}\right)\right] \quad (1)$$

where y'''_{Al} and y'''_{Mn} are the site fractions of Al and Mn in the third sublattice (Al, Mn)$_9$, respectively.

For the Al–Mg–Mn ternary system, the thermodynamic parameters for liquid and τ ($Mn_2Mg_3Al_{18}$) are adjusted with the measured phase diagram data. The Gibbs energy of the

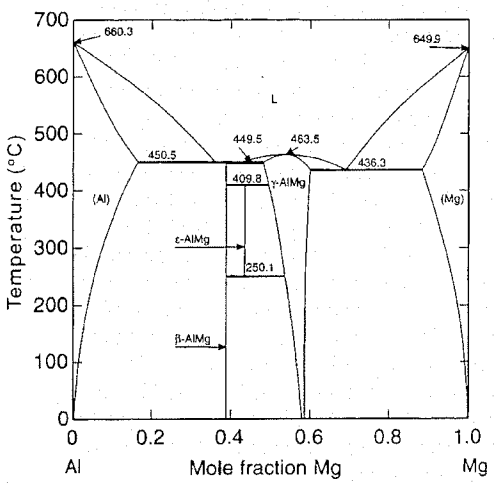

Fig. 2. Calculated Al–Mg phase diagram [1].

ternary liquid is described by Redlich-Kister polynomial [65]:

$$
\begin{aligned}
{}^{0}G_{m}^{L} &= x_{Al}\cdot {}^{0}G_{Al}^{L} + x_{Mg}\cdot {}^{0}G_{Mg}^{L} + x_{Mn}\cdot {}^{0}G_{Mn}^{L} \\
&\quad + R\cdot T(x_{Al}\cdot \ln x_{Al} + x_{Mg}\cdot \ln x_{Mg} + x_{Mn}\cdot \ln x_{Mn}) \\
&\quad + x_{Al}\cdot x_{Mg}\cdot L_{Al,Mg}^{L} + x_{Al}\cdot x_{Mn}\cdot L_{Al,Mn}^{L} \\
&\quad + x_{Mg}\cdot x_{Mn}\cdot L_{Mg,Mn}^{L} + {}^{ex}G_{Al,Mg,Mn}^{L} \qquad (2)
\end{aligned}
$$

in which R is the gas constant, and x_{Al}, x_{Mg}, and x_{Mn} are the mole fractions of Al, Mg and Mn, respectively. The standard element reference (SER) state [66], i. e. the stable structure of the element at 25 °C and 1 bar, is used as the Gibbs energy reference state. The parameters denoted $L_{i,j}^{L}$ are the interaction parameters from the binary systems. The excess Gibbs energy ${}^{ex}G_{Al,Mg,Mn}^{L}$ is expressed as follows:

$$
\begin{aligned}
{}^{ex}G_{Al,Mg,Mn}^{L} &= x_{Al}\cdot x_{Mg}\cdot x_{Mn} \\
&\times (x_{Al}\cdot {}^{0}L_{Al,Mg,Mn}^{L} + x_{Mg}\cdot {}^{1}L_{Al,Mg,Mn}^{L} + x_{Mn}\cdot {}^{2}L_{Al,Mg,Mn}^{L}) \qquad (3)
\end{aligned}
$$

The Gibbs energy of ternary compound t relative to the pure elements is expressed by the following expression:

$$
G_{m}^{\tau} - \frac{18}{23}\cdot G_{Al}^{0,fcc\_A1} - \frac{3}{23}\cdot G_{Mg}^{0,hcp\_A3} - \frac{2}{23}\cdot G_{Mn}^{0,cbcc\_A12} = A + B\cdot T \qquad (4)
$$

in which the coefficients A and B are assessed from the experimental phase diagram data. The parameters, G_{Al}^{0,fcc_A1}, G_{Mg}^{0,hcp_A3}, and $G_{Mn}^{0,cbcc\_A12}$, are the Gibbs energies of fcc_A1 Al, hcp_A3 Mg, and cbcc_A12 Mn, respectively.

The transition between disordered bcc_A2 and ordered bcc_B2 is not included in the present modeling since no evident experimental proof exists for such a transition, as mentioned by Liu et al. [40].

4.2. First-principles calculation

Density functional theory (DFT) calculations within the generalized gradient approximation (GGA) [67], as implemented in the highly efficient Vienna ab initio simulation package (VASP) [68–71], were utilized to calculate the enthalpy of formation for the $Mn_2Mg_3Al_{18}$ (τ) phase. The Perdew–Burke–Ernzerhof [72] GGA for the exchange-correlation potential was used for all the calculations, and the valence electrons were explicitly treated by projector augmented plane-wave (PAW) potentials. The ions were relaxed toward equilibrium until the Hellmann–Feynman forces were less than 10^{-2} eV · Å^{-1}. A plane-wave cutoff energy of 400 eV and an energy convergence criterion of 10^{-4} eV for electronic structure self-consistency were used in the calculations. Brillouin zone integrations were performed using the Monkhorst–Pack [73] k-point meshes scheme, and the total energy differences were converged to within 0.1 kJ · mol-atoms^{-1}. Both the unit cell sizes and the ionic coordinates were fully relaxed to find the stable state. The equilibrium enthalpy of formation, $\Delta H^{eq}(Mn_2Mg_3Al_{18})$, is given by the energy of $Mn_2Mg_3Al_{18}$ relative to the composition-weighted average of the energies of the pure constituents in their equilibrium crystal structures:

$$
\begin{aligned}
\Delta H^{eq}(Mn_2Mg_3Al_{18}) &= E(Mn_2Mg_3Al_{18}) \\
&- [x_A E^{eq}(Mg) + x_B E^{eq}(Mn) + x_C E^{eq}(Al)] \qquad (5)
\end{aligned}
$$

where $E(Mn_2Mg_3Al_{18})$, $E^{eq}(Mg)$, $E^{eq}(Mn)$ and $E^{eq}(Al)$ are the energies (per mole-atoms) of $Mn_2Mg_3Al_{18}$ and components, Al, Mg and Mn, respectively, and each is relaxed to its equilibrium geometry at zero-pressure. $x_i (i = A, B, C)$ is the atomic fraction of the component. And the reference states are fcc-Al (nonmagnetic), hcp-Mg (nonmagnetic), and αMn (collinear antiferromagnetic), respectively. The non-collinear antiferromagnetic αMn is not taken as the reference state due to the extensive computation time. According to the work of Hobbs et al. [74], the energy difference between collinear antiferromagnetic αMn and non-collinear antiferromagnetic αMn is negligibly small. Such a small energy difference will yield a negligible difference for the computed enthalpy of formation for the ternary $Mn_2Mg_3Al_{18}$ phase.

5. Results and discussion

The model parameters were evaluated using the computer-operated optimization program PARROT [75], which works by minimizing the square sum of the differences between measured and calculated values. The step-by-step optimization procedure carefully described by Du et al. [76] was utilized in the present assessment. The experimental data selected from the literature as well as the present experimental results are employed in the optimization. The optimized thermodynamic parameters are listed in Table 3. The first-principles calculated enthalpy of formation for τ is -10.2 kJ · mol-atoms^{-1}, which agrees reasonably with the value of -8.7 kJ · mol-atoms^{-1} resulting from the CALPHAD approach. The data predicted from the first-principles method can thus be taken as the good starting value for CALPHAD-type assessment.

Table 4 compares the numbers of the presently introduced parameters for individual phases with those of previous modeling [7]. In comparison with the previous modeling [7], fewer adjustable parameters are utilized in the present work. For example, 4 coefficients are used for describing the thermodynamic property of liquid instead of 5 [7]. In spite of this, a better agreement with the experimental data is obtained. In the present modeling, the liquid phase is first described with a regular solution model and then with a sub-regular solution model. The introduction of each parameter is justified by the corresponding experimental data. A similar procedure is used to model the other phases.

The complete Al–Mn phase diagram calculated using the present set of thermodynamic parameters is shown in Fig. 4. There is an inverse miscibility gap in the liquid phase with a minimum at 4227 K and x(Mn) = 0.29. The occurrence of such an inverse miscibility gap is not against the reliability of the thermodynamic parameters from the present modeling. Since at such high temperature, gas is stable instead of the liquid phase. Comparisons of the computed Al–Mn phase diagram with the corresponding experimental data are shown in Figs. 5 to 8. The fit to the ex-

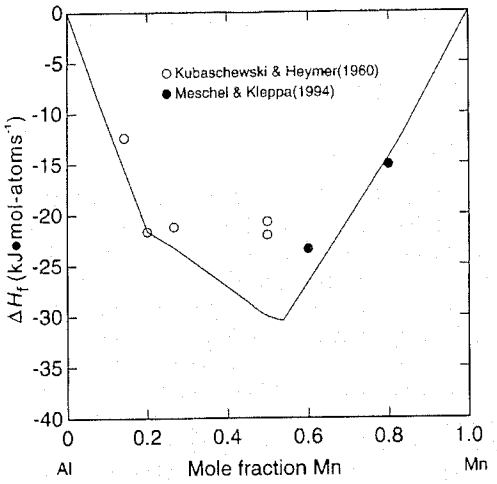

Fig. 9. Calculated and measured enthalpy of formation at 25 °C, compared with the experimental data [24, 35].

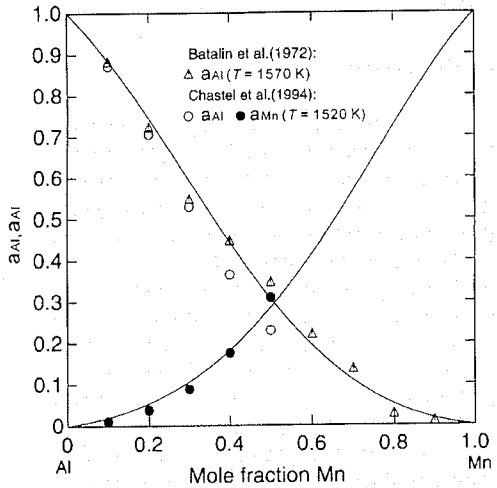

Fig. 10. Calculated activities of Al and Mn in the liquid at 1545 K, compared with the present experimental data [23, 37]. The reference states for both Al and Mn are liquid.

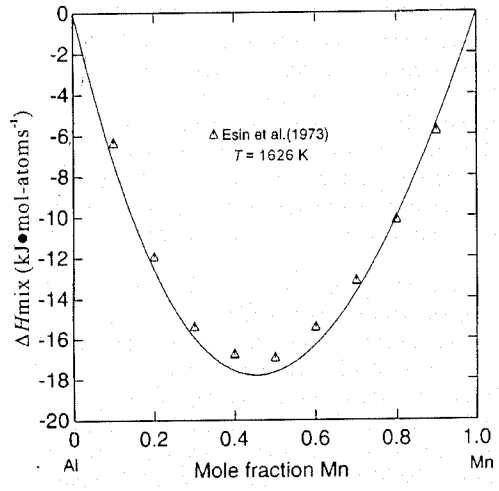

Fig. 11. Calculated enthalpy of mixing for the liquid at 1626 K along with the experimental data of Esin et al. [38].

perimental data is excellent. In particular, the measured liquidus temperatures in the composition range of 5 to 20 at.% Mn are well reproduced in the present modeling. This is not the case for previous calculations [6–8]. The presently observed melting behavior of λ-Al_4Mn is also well described by the modeling, as can be seen from Figs. 6 and 7.

In Fig. 9, the calculated enthalpies of formation at 25 °C are compared with the experimental values [24, 35]. The agreement with the experimental data of Meschel and Kleppa [24] is good within estimated experimental uncertainties. The old experimental values from Kubaschewski and Meymer [35] are considered to be only approximate due to the incompletion of the reactions, as mentioned by Kubaschewski and Meymer [35]. In the present modeling, the recent experimental data for the enthalpies of formation are utilized. Figure 10 shows a comparison of the computed activities of Al and Mn in liquid at 1545 K with the experimental data from Chastel et al. [23] and Batalin et al. [37]. The calculation can satisfactorily account for the experimental values. A further check on the reliability of the thermodynamic modeling in the Al–Mn binary system is provided by Fig. 11, where the calculated enthalpy of mixing for liquid at 1626 K is compared with the experimental values from Esin et al. [38]. It is demonstrated that these experimental data [38] are well described by the thermodynamic calculation.

In the following paragraphs, the computed Al–Mg–Mn ternary phase diagrams are compared with the experimental ones. For the Mg-rich side of the ternary system, only the experimental data, which are evaluated to be reliable by Ohno and Schmid-Fetzer [8], are used for such a comparison. In Fig. 12, the calculated isothermal sections of Mg-rich corner at several temperatures ranging from 730 to 670 °C are compared with the experimental values [43, 44, 47, 48]. The fit to the experimental data is excellent. Figure 13 shows the calculated solubility of Mn in liquid at a fixed Al composition, indicating also a good agreement with the experimental one [43, 48]. Figure 14 presents the computed monovariant line (L + (βMn) → Al_8Mn_5) along with the observed primary phases [47]. The primary phase regions and one data point corresponding to the simultaneous solidification of both (βMn) and Al_8Mn_5 are well reproduced by the modeling. However, one experimental datum on the primary Al_8Mn_5 cannot be described by the calculation. This datum is not consistent with the observed primary (βMn) region and double saturation of (βMn) and Al_8Mn_5. The calculated typical isothermal section at 710 °C is presented in Fig. 15 together with the measured tie lines between liquid and the precipitates [46, 47]. The measured compositions of the precipitates systematically indicate higher Al compared to the Al–Mn binary edge. It was suggested [8] that the accuracy of microprobe analysis of small precipitates could be inferior to those of binary Al–Mn data.

In Fig. 16, the computed isothermal sections at 450 and 400 °C in the Al-rich region are compared with the experimental data [56–58]. These experimental data are reasonably described by the present modeling. As shown by the dashed lines, the previous modeling [19] cannot describe the established phase equilibria, Al_6Mn + τ + (Al) and Al_6Mn + τ + λ-Al_4Mn. A comparison of the calculated joint solubility of Mg and Mn in (Al) with the experimental data [51] is made in Fig. 17. The small deviations between

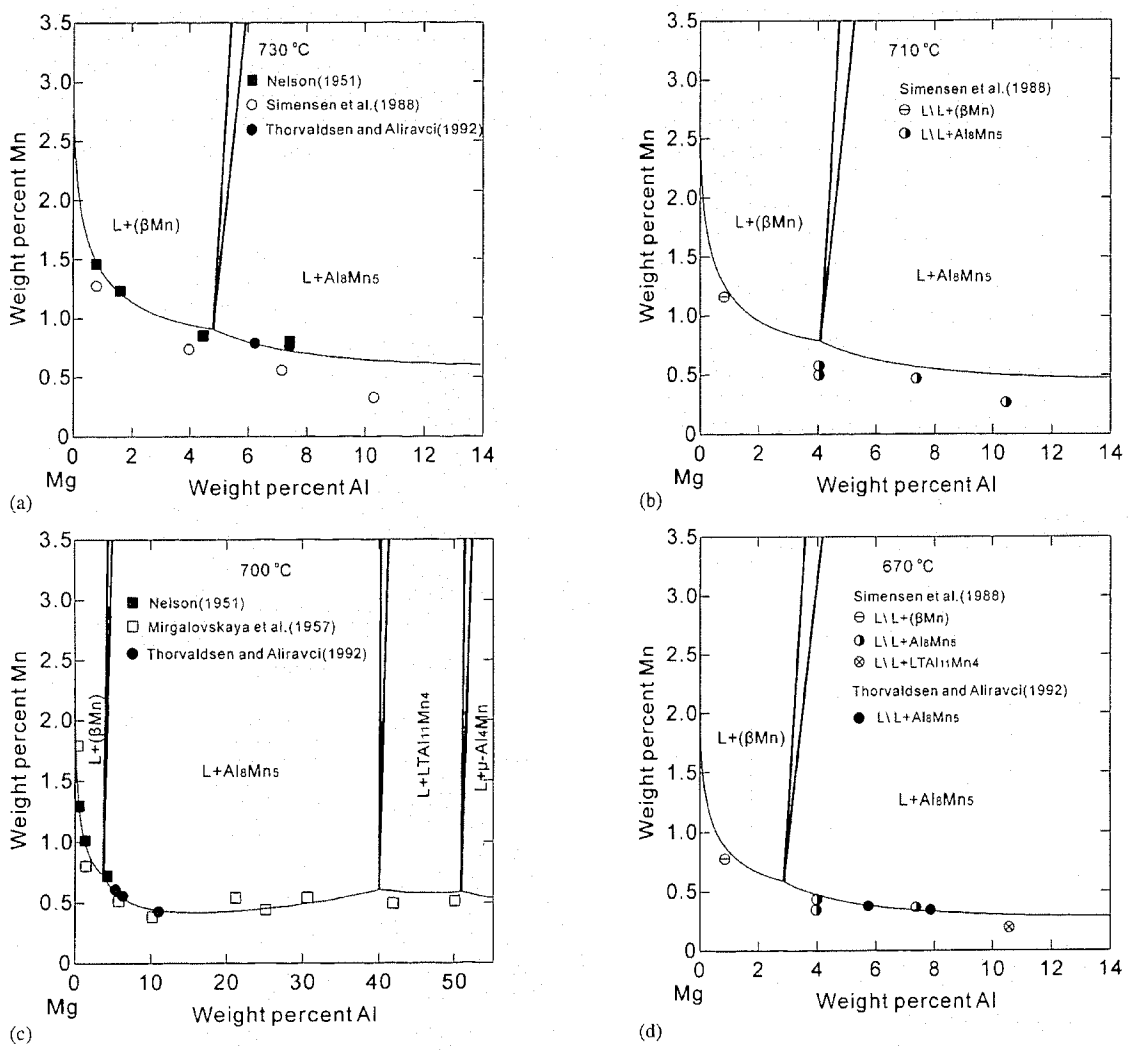

Fig. 12. Calculated isothermal sections in Mg-rich corner of the Al–Mg–Mn system, compared with the experimental data [43, 44, 47, 48]. (a) 730 °C, (b) 710 °C, (c) 700 °C, (d) 670 °C.

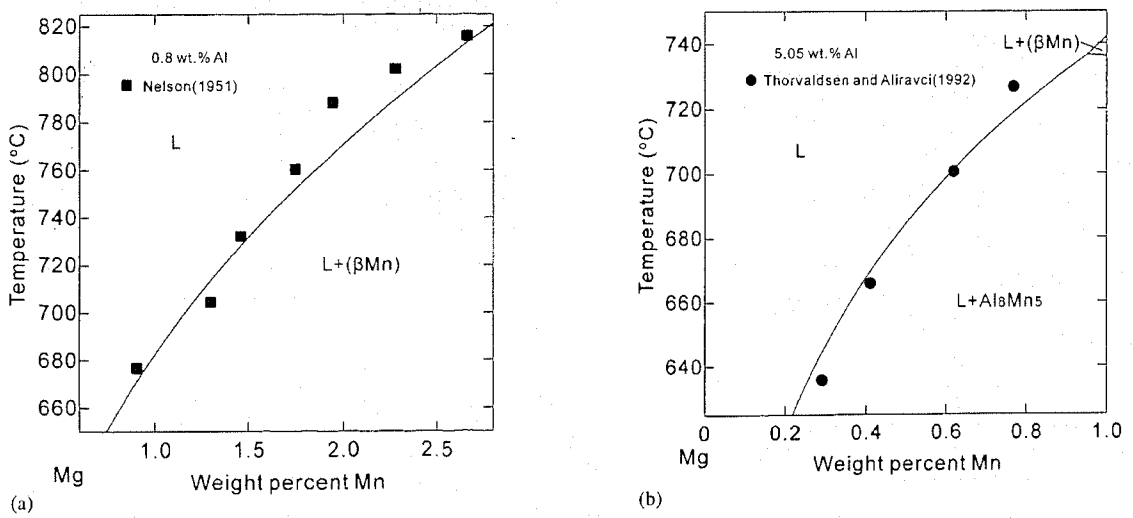

Fig. 13. Calculated solubility of Mn in liquid at a fixed Al composition in the Al–Mg–Mn system, compared with the experimental data [43, 48]. (a) 0.8 wt.% Al, (b) 5.05 wt.% Al.

calculation and experiment are traced to the differences between the calculated and measured solubilities of Mn in (Al) along the Al–Mn binary side.

The calculated liquidus projection in the whole composition is shown in Fig. 18. The observed primary phase regions [46–48] in the Mg-rich corner are compared with the calculated ones in Fig. 19a. It is demonstrated that the calculation can describe the primary phase regions. Figure 19b and c shows the detail of the calculated liquidus projection in Al-rich corner and the region close to the Al–Mg binary side, respectively. Figure 20 presents the reaction scheme for the whole Al–Mg–Mn system. Table 5 presents the invariant reactions according to the present modeling. The invariant reaction L ↔ (Al) + β-AlMg + τ observed by Barlock and Mondolfo [60] is confirmed by the present modeling. The computed reaction temperature is 451 °C, which agrees well with the measured one 447 °C [60]. Based on the early experimental data published in 1930s and 1940s, several four-phase equilibria were listed by Ran [18]. According to the work of Wakeman and Raynor [56] and Ohnishi et al. [57], all of the reactions recommended by Ran [18] are uncertain and might be metastable.

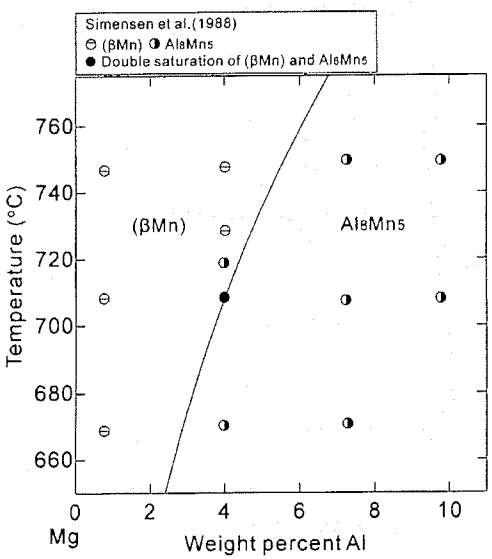

Fig. 14. Calculated monovariant line L + (βMn) → Al_8Mn_5 along with the experimental data [47] on primary phases. However, one experimental datum on the primary Al_8Mn_5 can not be described by the calculation. This datum is not consistent with the observed primary (βMn) region and double saturation of (βMn) and Al_8Mn_5.

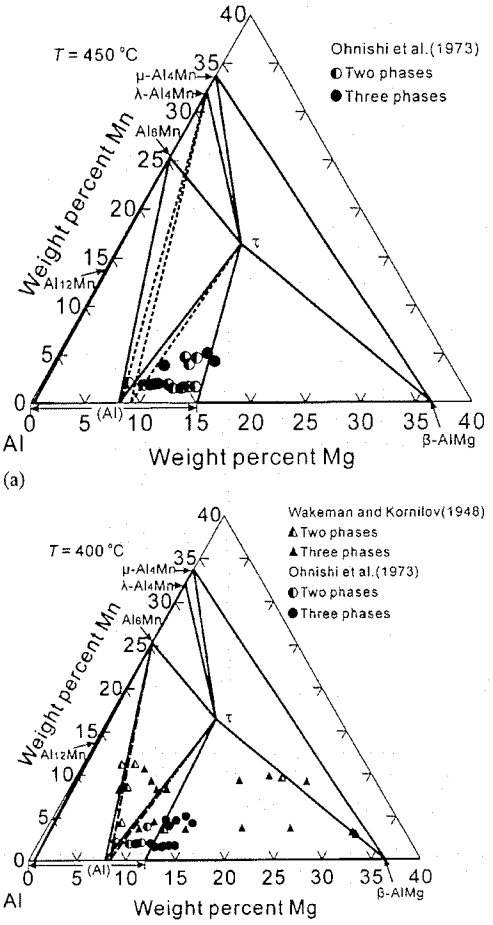

Fig. 16. Calculated isothermal sections together with the experimental data [56–58]. (a) 450 °C, (b) 400 °C.

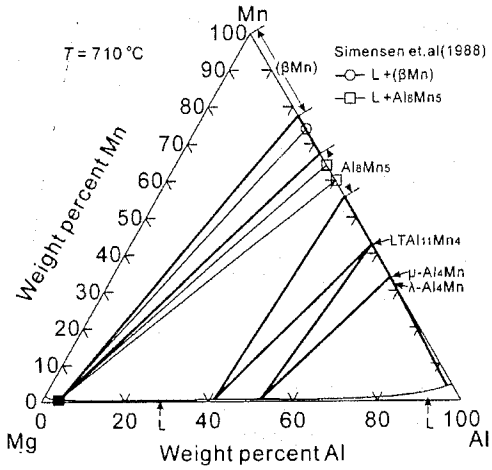

Fig. 15. Calculated isothermal section at 710 °C along with the experimental tie lines [46, 47].

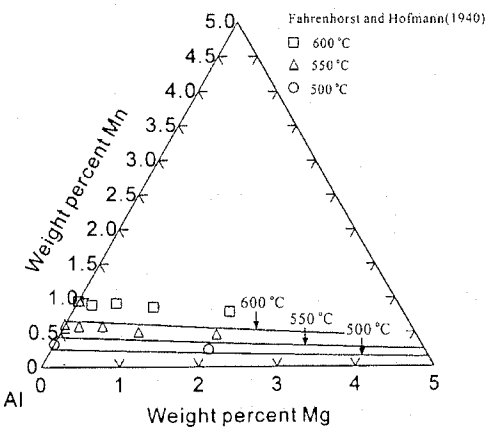

Fig. 17. Calculated joint solubility of Mg and Mn in (Al), compared with the experimental data [51].

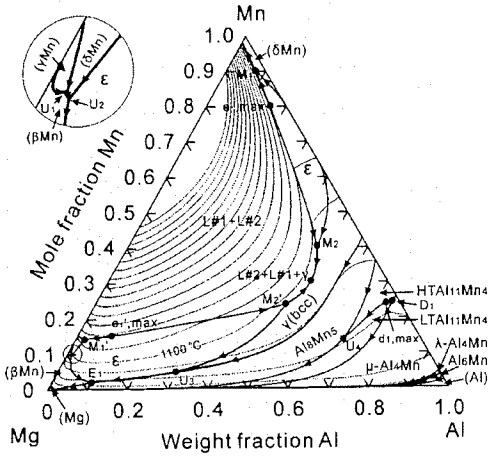

Fig. 18. Calculated liquidus projection for the whole Al–Mg–Mn system. The thick solid lines represent the monovariant lines, and the thin lines are isotherms.

This is confirmed by the present modeling. According to the present calculation, the ternary phase τ is formed via the peritectic reaction L + λ-Al_4 Mn + (Al) ↔ τ at 529 °C. The computed primary crystallization field for τ is extremely small. This agrees with the experimental observation [60]. Since experimental data for this ternary system are limited, especially in the Mn-rich corner, further experimental investigations are necessary to verify the calculated phase diagrams. The presently computed diagrams could be used for planning of new experiments.

6. Conclusions

- The phase equilibria in the Al-rich side of the Al–Mn system below 20 at.% Mn have been reinvestigated using 9 alloys, which are analyzed with XRD, DTA, optical microscopy and SEM/EDX techniques. It was found that in the absence of nucleation sites for λ-Al_4Mn the decomposition of Al_6Mn is retarded and superheating of Al_6Mn occurs at slow heating rates usually employed in DTA analysis. The DTA signals thus obtained for Al-rich AlMn-alloys are misleading to the interpretation yielding an invariant reaction Al_6Mn → μ-Al_4Mn + liquid. However, the true equilibrium reaction is Al_6Mn → λ-Al_4Mn + liquid, as found by equilibration plus quenching experiments.
- An optimal thermodynamic data set for the Al–Mn system was obtained by considering the present experimental results as well as critically evaluated literature data. The comprehensive comparison shows that the calculated phase diagram and thermodynamic properties are in very good agreement with the experimental information. Detectable improvements have been made, compared with the previous assessments.
- Phase equilibrium data of the Al–Mg–Mn system reported in the literature have been briefly reviewed. On the basis of reliable experimental data, a thermodynamic description for the ternary system was developed. Comprehensive comparisons show that the experimental data in both Al-rich and Mg-rich corners are well accounted for by the present description. The presented liquidus projection and reaction scheme establish the constitution of the Al–Mg–Mn system over wide temperature and composition ranges, which is of interest for engineering applications as well as basic materials research.

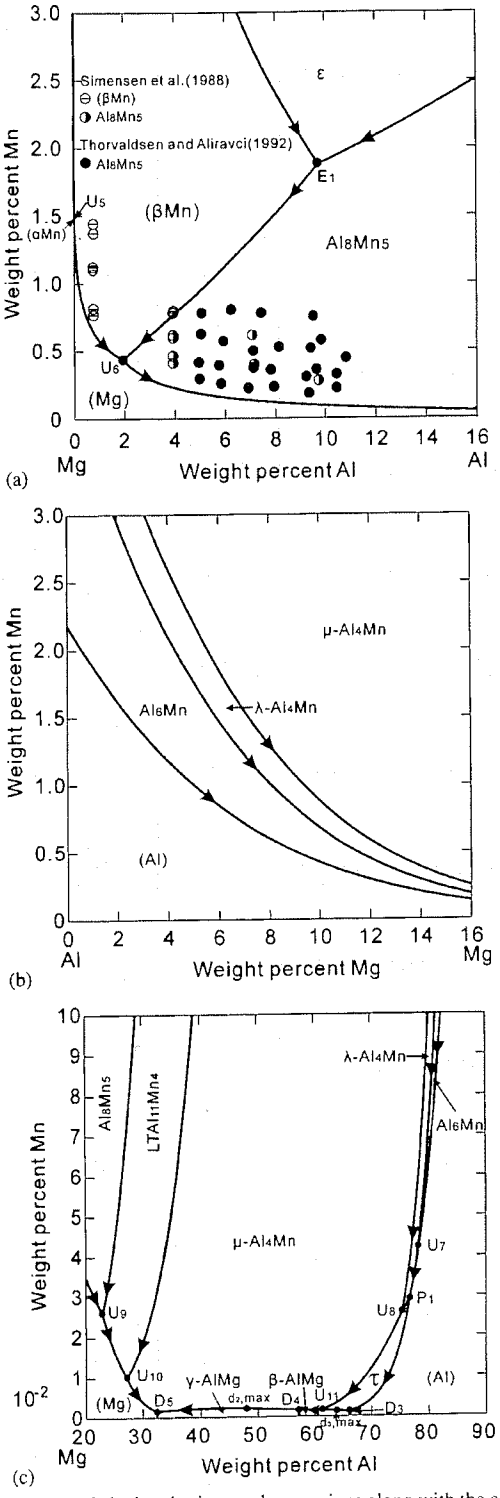

Fig. 19. Calculated primary phase regions along with the experimental data [46–48]. (a) Mg-rich corner, (b) Al-rich corner, (c) close to the Al–Mg binary side.

Table 5. Invariant equilibria in the Al–Mg–Mn system according to the present modeling (HT = $HTAl_{11}Mn_4$, and LT = $LTAl_{11}Mn_4$).

Reaction	T [°C]	Type	Phase	Composition (wt.%)		
				Al	Mg	Mn
L#2 + ε = (δMn) + L#1	1227	M_1	L#2	7	3	90
			ε	8.6	2.6	88.8
			δMn	7.4654	0.0559	92.4787
			L#1	2	84	14
L#1 + (γMn) = (δMn) + (βMn)	1081	U_1	L#1	0.898	89.2304	9.8716
			(γMn)	4.836	0.0206	95.1434
			(δMn)	5.7055	0.0266	94.2679
			(βMn)	5.1884	0.023	94.7886
L#1 + (δMn) = (βMn) + ε	1075	U_2	L#1	1.1437	89.3629	9.4934
			(δMn)	6.7955	0.0288	93.1757
			(βMn)	6.1578	0.0245	93.8178
			ε	7.6675	2.1052	90.2273
L#2 + ε = L#1 + γ	1058	M_2	L#2	47.3343	12.9886	39.6771
			ε	35.2784	2.21	62.5116
			L#1	47.7134	28.5337	23.7529
			γ	38.2464	0.2465	61.5071
L#1+ γ = Al_8Mn_5 + ε	922	U_3	L#1	28.4054	67.2064	4.3882
			γ	36.3275	0.147	63.5255
			Al_8Mn_5	39.2241	0	60.7759
			ε	33.718	1.9702	64.3118
HT = LT, μ, L#1	914.19	D_1	HT	57.494	0	42.506
			LT	57.4581	0	42.5419
			μ	66.268	0	33.732
			L#1	73.7947	1.4267	24.7786
L#1 + HT = Al_8Mn_5 + LT	905	U_4	L#1	66.7398	19.2531	14.007
			HT	56.1943	0	43.8057
			Al_8Mn_5	49.1832	0	50.8168
			LT	57.4581	0	42.5419
γ = (βMn) + Al_8Mn_5, ε	848.5	D_2	γ	29.972	0.0157	70.0123
			(βMn)	25.0634	0.0084	74.9281
			Al_8Mn_5	35.0187	0	64.9813
			ε	28.4515	0.311	71.2375
ε = L#1 + (βMn) + Al_8Mn_5	826	E_1	ε	28.0981	1.363	70.5389
			L#1	9.7322	88.3888	1.879
			(βMn)	24.669	0.0283	75.3027
			Al_8Mn_5	34.6397	0	65.3603
L#1 + (αMn) = (βMn) + (Mg)	650.6	U_5	L#1	0.0011	98.0932	1.9057
			(αMn)	0.0561	0.0005	99.9434
			(βMn)	0.7988	0.0005	99.2007
			(Mg)	0.0004	97.8522	2.1475
L#1 + (βMn) = (Mg) + Al_8Mn_5	639	U_6	L#1	2.1655	97.3637	0.4708
			(βMn)	21.1453	0.0036	78.8511
			(Mg)	0.6631	98.8715	0.4653
			Al_8Mn_5	31.7617	0	68.2383
L#1 + Al_6Mn = (Al) + λ	535	U_7	L#1	77.6157	22.3481	0.0362
			Al_6Mn	74.6631	0	25.3369
			(Al)	91.9267	7.9263	0.147
			λ	67.9077	0	32.0923
L#1 + λ + (Al) = τ	529	P_1	L#1	76.7157	23.2549	0.0294
			λ	67.9077	0	32.0923
			(Al)	91.5038	8.3679	0.1283
			τ	72.6552	10.9078	16.437
L#1 + λ = μ + τ	527	U_8	L#1	75.2993	24.675	0.0257
			λ	67.9077	0	32.0923
			μ	66.268	0	33.732
			τ	72.6552	10.9078	16.437
L#1 + Al_8Mn_5 = (Mg) + LT	516	U_9	L#1	23.4504	76.5199	0.0297
			Al_8Mn_5	41.5421	0	58.4579
			(Mg)	7.2495	92.7401	0.0104
			LT	57.4581	0	42.5419

Table 5. (continued)

Reaction	T [°C]	Type	Phase	Composition (wt.%)		
				Al	Mg	Mn
L#1 + LT = μ + (Mg)	482	U_{10}	L#1	27.8327	72.1558	0.0115
			LT	57.4581	0	42.5419
			μ	66.268	0	33.732
			(Mg)	9.2783	90.7183	0.0034
L#1, τ = (Al) + β-AlMg	450.5	D_3	L#1	66.1419	33.8568	0.0013
			τ	72.6552	10.9078	16.437
			(Al)	84.8158	15.1747	0.0095
			β-AlMg	63.5872	36.4128	0
L#1 + τ = μ + β-AlMg	450.3	U_{11}	L#1	60.845	39.1535	0.0015
			τ	72.6552	10.9078	16.437
			μ	66.268	0	33.732
			β-AlMg	63.5872	36.4128	0
L#1 = β-AlMg + γ-AlMg, μ	449.5	D_4	L#1	60.1341	39.8645	0.0014
			β-AlMg	63.5872	36.4128	0
			γ-AlMg	54.5507	45.4493	0
			μ	66.268	0	33.732
L#1 = (Mg) + γ-AlMg, μ	436.27	D_5	L#1	31.0114	68.9878	0.0008
			(Mg)	11.596	88.4038	0.0002
			γ-AlMg	39.94	60.06	0
			μ	80	0	20

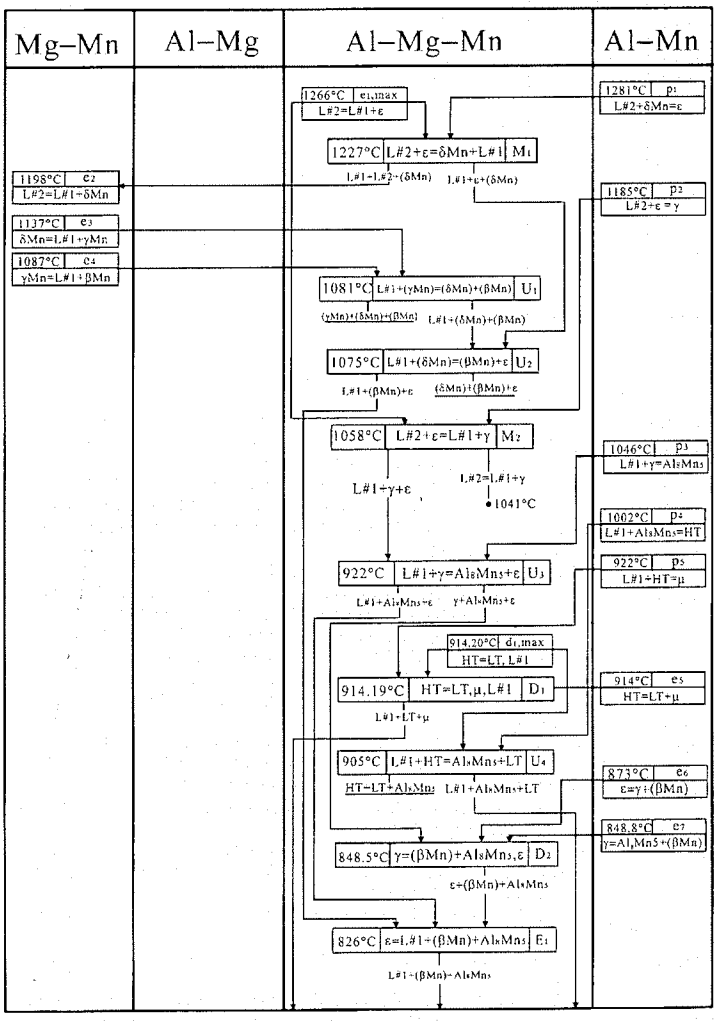

Fig. 20 (a)

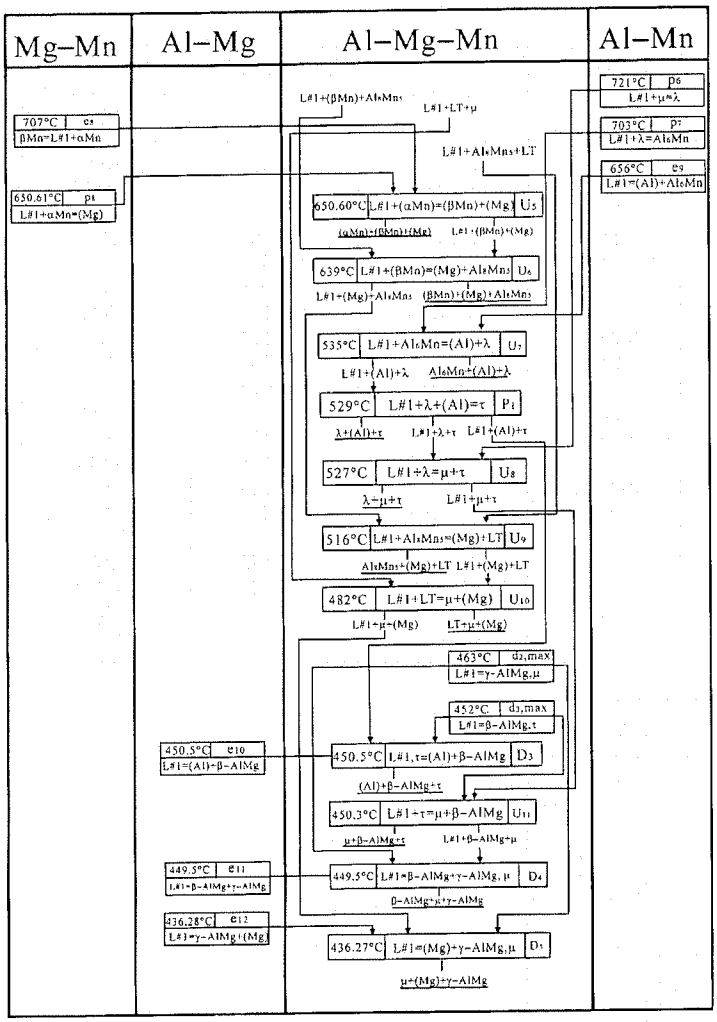

Fig. 20. Reaction scheme for the Al–Mg–Mn system according to the present work. HT = $HTAl_{11}Mn_4$, LT = $LTAl_{11}Mn_4$, $\lambda = \lambda - Al_4Mn$ and $u = u - Al_4Mn$.

(b)

The financial supports from the National Outstanding Youth Science Foundation of China (Grant No. 50425103) and the National Science Foundation of China (Grant No. 50323008) are greatly acknowledged. The financial support from Scientific and Technical Cooperation between Austria and China through OEAD project WTZ VII. B.9 is also appreciated. One of the authors (Yong Du) acknowledges Cheung Kong Scholars Program released by Ministry of Education of China. Thanks are also due to Professor X. J. Liu (Xiamen University, China) and Dr. X. Q. Chen (Oak Ridge National Laboratory, USA) for useful discussion.

References

[1] P. Liang, H.-L. Su, P. Donnadieu, M.G. Harmelin, A. Quivy, P. Ochin, G. Effenberg, H.-J. Seifert, H.L. Lukas, F. Aldinger: Z. Metallkd. 89 (1998) 536.
[2] J. Gröbner, D. Mirkovic, M. Ohno, R. Schmid-Fetzer: J. Phase Equilibria Diffusion 26 (2005) 234.
[3] P. Villars, L.D Calvert: Pearson's Handbook of Crystallographic Data for Intermetallic Phases, 2nd edition, ASM, Materials Park, Ohio, USA (1991).
[4] M. Ellner: Metall. Trans. A 21 (1990) 1669.
[5] G. Kreiner, H.F. Franzen: J. Alloy Compd. 261 (1997) 83.
[6] A. Jansson: Metall. Trans. A 23 (1992) 2953.
[7] X.J. Liu, I. Ohnuma, R. Kainuma, K. Ishida: J. Phase Equilibria 20 (1999) 45.
[8] M. Ohno, R. Schmid-Fetzer: Z. Metallkd. 96 (2005) 857.
[9] E.H. Dix, Jr. W.L. Fink, L.A. Willey: Trans. AIME 104 (1933) 335.
[10] T. Godecke, W. Koster: Z. Metallkd. 62 (1971) 727.
[11] M.C. Thornton: Unpublished research work, Alcan International Ltd, Banbury Laboratory, USA (1996).
[12] F. Weitzer, P. Rogl, F.H. Hayes, J.A.J. Robinson, in: F. Aldinger, H. Mughrabi (Eds.), Werkstoffwoche '96, Materialwissenschaftliche Grundlagen, Deutsche Gesellschaft für Materialkunde, Germany (1996) 185.
[13] M.A. Taylor: Acta Metall. 8 (1960) 256.
[14] J.L. Murray, A.J. McAlister, R.J. Schaefer, L.A. Bendersky, F.S. Biancaniello, D.L. Moffat: Metall. Trans. A 18 (1987) 385.
[15] J.A.J. Robinson, F.H. Hayes, A. Serneels, F. Weitzer, P. Rogl, in: I. Ansara (Ed.), COST 507 – definition of thermochemical and thermophysical properties to provide a database for the development of new light alloys, Vol. 1, COST Secretariat, Brussels, Belgium (1998) 230.
[16] J.D. Hanawalt, C.E. Nelson, J.A. Peloubet: Trans AIME (1942) 273.
[17] C.E. Nelson: Trans. Am. Foundrymen's Soc. (1948) 1.
[18] Q.S. Ran, in: G. Effenberg, F. Aldinger, L. Rokhlin (Eds.), Ternary alloys, Vol. 16, Graphischer Betrieb Konrad Triltsch, D-97070 Würzburg, Germany (1999) 292.
[19] I. Ansara, A.T. Dinsdale, M.H. Rand: COST 507, Thermochemical database for light metal alloys, Vol. 2, European communities, Luxembourg (1998) 325.
[20] A.J. McAlister, J.L. Murray: Bull. Alloy Phase Diagrams 8 (1987) 438.
[21] G.M. Kuznetsov, A.D. Barsukov, M.I. Abas: Sov. Non Ferrous Met. Res. 11 (1983) 47.
[22] Y. Minamino, T. Yamane, H. Araki, N. Takeuchi, Y.-S. Kang, Y. Miyamoto, T. Okamoto: Metall. Trans. A 22 (1991) 783.

[23] R. Chastel, M. Saito, C. Bergman: J. Alloy Compd. 205 (1994) 39.
[24] S.V. Meschel, O.J. Kleppa, in: J.S. Faulkner, R.G. Jordan (Eds.), NATO ASI Series, Series E: Applied Sciences, Vol. 256, Kluser Academic Publishers, The Netherlands (1994) 103.
[25] C. Sigli: CALPHAD XXIV conference, Kyoto, Japan (1995).
[26] M. Matuo, T. Muramatsu, A. Asanuma, S. Komatsu, K. Ikeda: Keikinzoku 47 (1997) 15.
[27] E.H. Dix, W.D. Keith: Proc. AIME, Inst. Metals Div. (1927) 315.
[28] E. Fahrenhorst, W. Hofmann: Metallwirtschaft 19 (1940) 891.
[29] H.W.L. Phillips: J. Inst. Met. 69 (1943) 275.
[30] E. Butchers, W. Hume-Rothery: J. Inst. Met. 71 (1945) 87.
[31] I. Obinata, E. Hata, K.Yamaji: Nippon Kinzoku Gakkaishi 17 (1953) 496.
[32] H. Kono: J. Phys. Soc. Japan 13 (1958) 1444.
[33] A.J.J. Koch, P. Hokkeling, M. G. v.d. Steeg, K.J. Devos: J. Appl. Phys. 31 (1960) 75S.
[34] W. Köster, E. Wachtel: Z. Metallkd. 51 (1960) 271.
[35] O. Kubaschewski, G. Meymer: Trans. Faraday Soc. 6 (1960) 473.
[36] M.E. Drits, E.S. Kadaner, E.M. Padezhnova, N.R. Bochvar: Russ. J. Inorg. Chem. 9 (1964) 759.
[37] G.I. Batalin, E.A. Beloboradova, B.A. Stukalo, A.A. Chekhovskii: Sov. Prog. Chem. 38 (1972) 83.
[38] Y.O. Esin, N.T. Bobrov, M.S. Petrushevskii, P.V. Gel'd: Russ. J. Phys. Chem. 47 (1973) 1103.
[39] R.J. Kematick, C.E. Myers: J. Alloys Compd. 178 (1992) 343.
[40] X.J. Liu, R. Kainuma, H. Ohtani, K. Ishida: J. Alloys Compd. 235 (1996) 256.
[41] A. Beerwald: Metallwirtschaft 23 (1944) 404.
[42] N.V.Ageev, I.I. Kornilov, A.N. Khlapova: Izv. Inst. Fiz-Khim. Anal. 14 (1948) 130.
[43] B.J. Nelson: J. Metals 3 (1951) 797.
[44] M.S. Mirgalovskaya, L.N. Matkova, E.M. Komova: Trudy Inst. Met. Im. A.A. Baikova, Akad. Nauk 2 (1957) 139.
[45] B.C. Oberlander, C.J. Simensen, J. Svalestuen: Conf. Magnesium Technology, Inst. of Metals (1986) 133.
[46] C.J. Simensen. B.C. Oberlander, J. Svalestuen, A. Thorvaldsen: Z. Metallkd. 79 (1988) 537.
[47] C.J. Simensen, B.C. Oberlander, J. Svalestuen, A. Thorvaldsen: Z. Metallkd. 79 (1988) 696.
[48] A. Thorvaldsen, C.A. Aliravci: Adv. Prod. Fabr. Light Met. Met. Matrix Comp. Proc. Int. Symp. (1992) 277.
[49] W.G. Leemann: Aluminium Arch. 9 (1938) 6.
[50] W. Hofmann: Aluminium (1938) 865.
[51] E. Fahrenhorst, W. Hofmann: Metallwirtschaft 19 (1940) 891.
[52] E. Butchers, G.V. Raynor, W. Hume-Rothery: J. Inst. Met. 69 (1943) 209.
[53] A.T. Little, G.V. Raynor, W. Hume-Rothery: J. Inst. Met. 69 (1943) 423.
[54] L.F. Mondolfo: John Wiley and Sons, Inc., New York (1943) 100.
[55] E. Butchers, W. Hume-Rothery: J. Inst. Met. 71 (1945) 291.
[56] D.W. Wakeman, G.V. Raynor: J. Inst. Met. 75 (1948) 131.
[57] T. Ohnishi, Y. Nakatani, K. Shimizu: Light Metals Tokyo 23 (1973) 202.
[58] T. Ohnishi, Y. Nakatani, K. Shimizu: Light Metals Tokyo 23 (1973) 437.
[59] H.-K. Fun, H.-C. Lin, T.-J. Lee, B.-C. Yipp: Acta Crystallogr. C 50 (1994) 661.
[60] J. G. Barlock, L.F. Mondolfo: Z. Metallkd. 66 (1975) 605.
[61] M.A. Taylor: Acta Crystallogr. 14 (1961) 84.
[62] N.Kh. Abrikosov, L. Ivanova, V.A. Danil'chenko: Inorg. Mater. 7 (1971) 933.
[63] M. Hillert, L.-I. Staffansson: Acta Chem. Scand. 24 (1970) 3618.
[64] J.O. Andersson, A.F. Guillermet, M. Hillert, B. Jansson, B. Sundman: Acta Metall. 34 (1986) 437.
[65] O. Redlich, A.T. Kister: Ind. Eng. Chem. 40 (1948) 345.
[66] A.T. Dinsdale: Calphad 15 (1991) 317.
[67] J.P. Perdew, Y. Wang: Phys. Rev. B 45 (1992) 13244.
[68] G. Kress, J. Hafner: Phys. Rev. B 47 (1993) 558.
[69] G. Kress, J. Furthmuller: J. Phys. Rev. B 54 (1996) 1169.
[70] D. Vanderbit: Phys. Rev. B 41 (1990) 7892.
[71] G. Kress, J. Hafner: J. Phys. Condes. Matter. 6 (1994) 8245.
[72] J.P. Perdew, K. Burke, M. Ernzerhof: Phys. Rev. Lett. 77 (1996) 3865.
[73] H.J. Monkhorst, J.D. Pack: Phys. Rev. B 13 (1972) 5188.
[74] D. Hobbs, J. Hafner, D. Spisak: Phys. Rev. B 68 (2003) 01447-1.
[75] B. Sundman, B. Jansson, J.O. Andersson: Calphad 9 (1985) 153.
[76] Y. Du, R. Schmid-Fetzer, H. Ohtani: Z. Metallkd. 88 (1997) 545.

(Received April 10, 2007; accepted July 5, 2007)

Bibliography

DOI 10.3139/146.101547
Int. J. Mat. Res. (formerly Z. Metallkd.)
98 (2007) 9; page 855–871

ISSN 1862-5282

Correspondence address

Professor Dr. Yong Du
State Key Laboratory of Powder Metallurgy
Central South University, Changsha, Hunan 410083, P.R. China
Tel.: +86 731 8836213
Fax: +86 731 8710855
E-mail: yong-du@mail.csu.edu.cn

You will find the article and additional material by entering the document number MK101547 on our website at www.ijmr.de